Published in final edited form as:
Biochemistry. 2011 April 5; 50(13): 2478–2485. doi:10.1021/bi101864k.

Partitioning of Synaptotagmin I C2 Domains between Liquid-Ordered and Liquid-Disordered Inner Leaflet Lipid Phases†

Chen Wan[1,2], **Volker Kiessling**[1,2], **David S. Cafiso**[1,3], and **Lukas K. Tamm**[1,2,*]

[1]Center for Membrane Biology, University of Virginia, Snyder building, P.O. Box 800886, Virginia 22908

[2]Department of Molecular Physiology and Biological Physics, University of Virginia, Snyder building, P.O. Box 800886, Virginia 22908

[3]Department of Chemistry, University of Virginia, Snyder building, P.O. Box 800886, Virginia 22908

Abstract

Synaptotagmin I is the calcium sensor in synchronous neurotransmitter release by fusion of synaptic vesicles with the presynaptic membrane in neurons. Synaptotagmin I interacts with acidic phospholipids, but also with SNAREs at various stages in presynaptic membrane fusion. Since SNAREs can be organized into small cholesterol-dependent clusters in membranes, it is important to determine whether the C2 domains of synaptotagmin target membrane domains of different cholesterol content. To address this question, we used a previously developed asymmetric two-phase lipid bilayer system to investigate the membrane binding and lipid phase targeting of soluble C2A and C2AB domains of synaptotagmin. We found that both domains target more disordered cholesterol-poor domains better than highly ordered cholesterol-rich domains. The selectivity is greatest (~3 fold) for C2A binding to disordered domains that are formed in the presence of 5 mol% PIP_2 and 15 mol% PS. It is smallest (~1.4 fold) for C2AB binding to disordered domains that are formed in the presence of 40 mol% PS. In the course of these experiments, we also found that C2A domains in the presence of Ca^{2+} and C2AB domains in the absence of Ca^{2+} are quite reliable reporters of acidic lipid distribution between ordered and disordered lipid phases. Accordingly, PS prefers the liquid-disordered phase about two-fold over the liquid-ordered phase, but PIP_2 has an up to three-fold preference for the liquid-disordered phase.

Ca^{2+}-triggered membrane fusion of synaptic vesicles with the presynaptic plasma membrane of neurons is the central event in synaptic transmission. This process is tightly regulated by synaptotagmin I (syt I)[1], soluble *N*-ethylmaleimide-sensitive factor attachment receptor (SNARE) proteins and other factors (1-3). Assembly of the four helix bundle SNARE

†This work was supported by NIH grant P01 GM072694.

* To whom correspondence should be addressed. Phone: (434) 982-3578. Fax: (434) 243-8271. lkt2e@virginia.edu.

Supporting Information: One figure demonstrating the coupling of lipid phases between outer and inner leaflets in two-phase lipid bilayers. The supplemental materials may be accessed free of charge online at http://pubs.acs.org.

[1]Abbreviations: bPC, porcine brain phosphatidylcholine; bSM, porcine brain sphingomyelin; bPE, porcine brain phosphatidylethanolamine; $bPIP_2$, brain phosphatidylinositol 4,5-bisphosphate; Chol, cholesterol; DPS, 1,2-dimyristoyl phophatidylethanolamine-*N*-[poly(ethylene glycol)-triethoxysilane]; EGTA, ethylene glycol bis(β-aminoethylether)*N*,*N*′-tetraacetic acid; NBD-DPPE, 1,2-dipalmitoyl phosphatidylethanolamine-*N*-[7-nitro-2-1,3-benzoxadiazol-4-yl]; POPS, 1-palmitoyl-2-oleoyl phosphatidylserine; Rh-DPPE, 1,2-dipalmitoyl phosphatidylethanolamine-*N*-(lissamine rhodamine B sulfonyl); syt I, synaptotagmin I; syt I C2AB, soluble fragment of synaptotagmin I containing the C2A and C2B domains; syt I C2A, C2A domain of syt I; syt I C2B, C2B domain of syt I; SNARE, soluble *N*-ethylmaleimide-sensitive factor attachment receptor; SNAP-25, synaptosomal-associated protein of 25 kDa; TIRFM, total internal reflection fluorescence microscopy; TM, transmembrane.

protein complex docks the vesicles to the presynaptic membrane and is believed to be the essential reaction that drives membrane fusion (4-8). Syt I is an integral membrane protein of synaptic vesicles and is the Ca^{2+} sensor for synchronous neurotransmitter release (9-13). It is anchored to the membrane by a single transmembrane domain near the N-terminus and contains two C2-type Ca^{2+}-sensing domains (C2A and C2B) towards its C-terminal end (14). A long linker connects C2A to the TM domain and a short linker connects C2A and C2B. C2A and C2B have similar folds consisting of a β-sandwich formed from two 4-stranded β-sheets. The loops that connect the β-strands protruding from one end form binding sites for Ca^{2+} ions, binding three or two Ca^{2+} ions, respectively. Ca^{2+} bound to these loops mediates the binding of C2 domains to negatively charged membrane surfaces (15, 16). In general, syt I C2 domains can interact with the synaptic vesicle membrane (cis-membrane) as well as with the presynaptic plasma membrane (trans-membrane) (17). In the following we will only consider the trans-bilayer-interactions.

The C2 domains of syt I have been proposed to regulate fusion through interaction with acidic phospholipids such as phosphatidylserine (PS) and phosphatidylinositol (PI) and its phosphorylated derivatives by binding and penetrating into the presynaptic membrane surface upon Ca^{2+} binding (18-20). In fact, when expressed as independent domains, the two C2 domains have been reported to prefer different membrane compositions. The membrane binding of C2A and C2B are strongly Ca^{2+}-dependent and they bind well to bilayers composed of negatively charged lipids. However, C2A has a preference for PC/PE and PS containing bilayers, while C2B prefers to bind to bilayers containing PIP_2. C2B even binds weakly in the absence of Ca^{2+} to PC/PE/PS or PC/PE/PIP_2 bilayers through a highly basic strand in its β-sandwich (21-23). When expressed as tandem C2A and C2B domains, the two domains reinforce each other's binding and membrane penetration behavior (24). Expressed C2A and C2B have also been reported to change membrane curvature (25) and full-length syt I co-reconstituted with SNAREs can enhance SNARE-mediated fusion under appropriate conditions (26, 27). However, exactly how syt I co-operates with SNAREs and thereby imparts Ca^{2+} control on neuronal exocytosis is not yet fully understood.

The SNAREs syntaxin 1A and SNAP-25 concentrate in partially overlapping clusters in plasma membranes that are also the sites of exocytosis in neuroendocrine cells (28) and pancreatic β cells (29). Cholesterol depletion disperses these clusters in plasma membranes and simultaneously impairs exocytosis. Although these clusters are cholesterol-dependent, SNAREs are not found in detergent-resistant fractions and therefore, are unlikely targeted to “rafts” in cell membranes. These results raise the question of whether syt I C2 domains prefer cholesterol-rich or cholesterol-poor regions of the plasma membrane and whether regulation of such partitioning could regulate potential interactions with SNAREs. Since C2 domains target the cytoplasmic (inner) leaflets of plasma and intracellular membranes, one strategy to answer this question is to use model membranes with coexisting liquid-ordered (l_o) and liquid-disordered (l_d) domains and inner leaflet lipid compositions. Unlike mixtures of PC, SM, and cholesterol, typical inner leaflet lipid mixtures of PC, PE, PS and cholesterol do not form phase-separated l_o and l_d phases on their own in model membranes (30, 31). However, such domains can be induced to form by phase coupling adjacent to phase-separated l_o-l_d domains formed by outer leaflet lipid PC, SM, and cholesterol mixtures in asymmetric supported lipid bilayers (30, 32).

In the current work, we investigate the Ca^{2+}-dependent binding and surface distribution of syt I C2A and C2AB on asymmetric bilayers with induced coexisting l_o-l_d phases, as well as the Ca^{2+}-independent binding of C2AB on these bilayers as a function of the concentrations of the anionic lipids PS and PIP_2 and the curvature-inducing lipid PE in the inner leaflet. We find that under all lipid conditions, C2 domains favor l_d over l_o lipid phases in the presence and absence of Ca^{2+}. C2A's binding preference for l_d phases is independent of the PS

concentration, probably reflecting a concentration-independent partitioning of this lipid between ordered and disordered phases. However, C2A partitioning between l_o and l_d lipid phases depends on the PIP_2 concentration, indicating a progressively higher accumulation of PIP_2 in disordered membrane regions as PIP_2 and C2A levels are increased. The selectivity of C2AB for disordered membrane regions is not as high as that of C2A and, importantly, C2AB in the absence of Ca^{2+}can be used as a reliable reporter of acidic lipid partitioning between inner leaflet l_d and l_o phases in asymmetric lipid bilayers.

Materials and Methods

The following materials were purchased and used without further purification: POPS, bPC, bSM, bPE, $bPIP_2$, NBD-DPPE, Rh-DPPE (Avanti Polar Lipids, Alabaster, AL); Alexa Fluor 546 C_5-maleimide (Invitrogen, Carlsbad, CA); cholesterol, HEPES, and glycerol (Sigma Chemical, St. Louis, MO); chloroform, ethanol, methanol, ether, Contrad detergent, all inorganic salts, acids, bases and hydrogen peroxide (Fisher Scientific, Fair Lawn, NJ). DPS was custom synthesized by Shearwater Polymers (Huntsville, AL). Water was purified first with deionizing and organic-free filters (Virginia Water Systems, Richmond, VA) and then with a NANOpure system from Barnstead (Dubuque, IA) to achieve a resistivity of 18.2 MΩ/cm. The following buffers were used for vesicle preparation and protein binding: HKE buffer (25 mM HEPES, 100 mM KCl, 1 mM EGTA, pH 7.4) and HKC buffer (25 mM HEPES, 100 mM KCl, 1 mM $CaCl_2$, pH 7.4). Synaptotagmin I C2A and C2AB lacking the transmembrane domains were prepared as described (19, 33).

Large Unilamellar Vesicles (LUVs)

The desired lipids were codissolved in chloroform or chloroform/methanol. Solvent was evaporated under a stream of N_2 gas, using a rotary evaporator when PIP_2 was present. After drying 1h in vacuum, the resulting residue was suspended in HKE buffer, rapidly vortexed, freeze-thawed five times by alternate submersion in liquid N_2 and then a water bath at 40 °C, and then extruded by 15 passes through two polycarbonate membranes with a pore diameter of 100 nm (Avestin, Ottawa, ON). Vesicles were stored at 4 °C for not more than 5 days before use.

Quartz Slides

Slides ($40\times25\times1$ mm^3) were purchased from Quartz Scientific (Fairport Harbor, OH). They were cleaned by boiling in Contrad detergent for 10 mins and then sonicated while still in detergent for 30 mins, followed by extensive rinsing with water, methanol, and water again. Remaining organic residues were removed by immersion in three volumes of sulfuric acid to one volume of 30% hydrogen peroxide, followed by extensive rinsing in water. Immediately prior to use, slides were further cleaned for 10 mins in an argon plasma sterilizer (Harrick Scientific, Ossining, NY).

Tethered Polymer-Supported Bilayers

The bilayers were formed as illustrated in Figure 1 by a combined Langmuir-Blodgett/ Vesicle Fusion (LB/VF) technique (34-36). A lipid monolayer containing 3% DPS was spread from a chloroform solution onto a pure water surface in a Nima 611 Langmuir-Blodgett trough (Nima, Conventry, U.K.). The solvent was allowed to evaporate for 10 mins, and the monolayer was compressed at a rate of 10 cm^2/min to reach a surface pressure of 32 mN/m and equilibrated for 5 to 10 mins. A clean quartz slide was then rapidly (200 mm/min) dipped into the trough and slowly (5 mm/min) withdrawn, while a feedback circuit maintained a constant surface pressure and monitored the transfer of lipids onto the substrate by measuring the change in surface area. The resulting monolayer on the solid support is known as the LB monolayer. The DPS molecules were tethered to the surface by drying the

coated slides in a desiccator at room temperature overnight and subsequently curing them in a 70 °C oven for 40 mins. The slide was transferred to a desiccator, allowed to equilibrate at room temperature, and typically used on the same day.

Slides with tethered polymer supported LB monolayers were placed in a custom built flow-through chamber. A 0.1 mM suspension of large unilamellar vesicles in HKE buffer was slowly and carefully injected into the chamber to avoid washing away the LB monolayer, and then incubated for 35 mins. Excess vesicles were washed out by extensive rinsing with HKE buffer. Inner leaflet monolayers containing 40% POPS required 1 mM $CaCl_2$ during vesicle fusion for reproducible bilayer formation.

Fluorescence Labeling of Synaptotagmin I C2 Domains

Both synaptotagmin I C2A and C2AB domains used in this study had single cysteine mutations (syt I C2A L142C and syt I C2AB E269C) for labeling with Alexa Fluor 546. The labeled cysteine residues are exposed to the aqueous environment far away from the membrane binding loops (19, 33). We therefore don't expect any fluorescence intensity changes due to insertion of the fluorophores into the lipid bilayer. Syt I C2 domains were dissolved in a degassed 10 mM HEPES buffer (pH 7.0), a 10-fold molar excess of *tris*(2-carboxylethyl)phosphine (TCEP) was added, and the solution was incubated at room temperature for 2 hours. 1 mg/ml Alexa Fluor 546 (10 mM HEPES, pH 7.4) was added to yield a dye/protein ratio of 10:1 (mol:mol) and incubated at 4 °C overnight. Unreacted dyes were removed by Sephadex G-50 gel filtration in 10 mM HEPES buffer (pH 7.0). Labeling efficiencies between 30 and 90% were obtained as determined by absorbance spectroscopy using the extinction coefficient of Alexa Fluor 546 (93,000 M^{-1} cm^{-1}).

Epifluorescence Microscopy

Images were recorded on a Zeiss Axiovert 200 fluorescence microscope (Carl Zeiss, Thornwood, NY) with a mercury lamp as light source, a 63× water immersion objective (Zeiss; NA = 0.95), and an electron multiplying charge-coupled device (EMCCD) cooled to -70°C (iXon DV887ESC-BV; Andor, Belfast, UK) as a detector. Images were acquired using homemade software written in LabVIEW (National Instruments, Austin, TX). Bilayers stained with NBD-DPPE were illuminated through a 480 nm band-pass filter (D480/30, Chroma, Brattleboro, VT) and via a dichroic mirror (505dclp, Chroma) through the objective. Fluorescence was observed through a 535 nm band-pass filter (D535/40, Chroma). Alexa Fluor 546 C5-maleimide labeled protein layers were illuminated through a 540 nm band-pass filter (D540/25, Chroma) and via a dichroic mirror (565dclp, Chroma) through the objective. Fluorescence was observed through a 605 nm band-pass filter (D605/55, Chroma).

Total Internal Reflection Fluorescence Microscopy (TIRFM)

A Zeiss Axiovert 35 fluorescence microscope (Carl Zeiss, Thornwood, NY) with an argon ion laser beam (Innova 300C; Coherent, Palo Alto, CA) as light source and a 40× water immersion objective (Zeiss; NA = 0.75) was used for TIRFM. Fluorescence images of 128 × 128 $pixel^2$ were recorded through a 610 nm band pass filter (D610/60, Chroma, Brattleboro, VT) by an EMCCD cooled to -70°C (iXon DU-860E-CSO-#BV; Andor, Belfast, UK) and acquired using homemade software written in LabVIEW (National Instruments, Austin, TX). To monitor the Alexa Fluor 546 labeled protein layer, the focused laser beam was tuned to 514 nm and directed through a trapezoidal prism onto the quartz-buffer interface where the supported bilayer was attached. The prism-quartz interface was lubricated by glycerol to allow easy translocation of the sample chamber on the microscope stage. The laser beam was totally internally reflected at an angle of 72° from the surface normal, producing an evanescent wave that decays exponentially in the solution with a characteristic

penetration depth of ~100 nm in our setup. An elliptical area of about 250 μm × 65 μm was illuminated and observed. The intensity of the laser beam was computer-controlled through an acousto-optic modulator (AOM-40, IntraAction, Bellwood, IL) or could be completely blocked by a computer-controlled shutter (Vincent Associates, Rochester, NY).

Binding of Synaptotagmin I C2 Domains to Supported Bilayers

Two ml of a 0.2 μM Alexa Fluor 546 labeled syt I C2 domain solution (HKE or HKC buffer) was injected into the flow-through chamber containing an asymmetric supported bilayer. The binding process was monitored for 15-20 min by TIRFM and the images were recorded every 30 s. Multiple images from surrounding areas were taken after binding was completed. Excess protein was washed away by 10 volumes of HKE or HKC buffer. Polarized TIRFM (37, 38) experiments revealed that the fluorescence intensities from different phases is proportional to the amount of protein binding. Comparing images acquired under s- and p-polarized excitation light showed that the influence of the fluorophore orientation can be neglected (data not shown).

Image Analysis

Images of the protein layer were analyzed by homemade programs written in LabVIEW (National Instruments). The mean intensities from domain regions and non-domain regions were extracted separately and the binding curves of those regions were reconstructed. The intensity ratios of domain over non-domain regions were calculated from the extracted intensities of domain and adjacent non-domain regions. Typically, 10-20 ratios were obtained for each image and 10-30 images were taken for each condition after binding saturated. The mean ratios, standard deviations and standard errors (the standard deviations of the mean) were then calculated accordingly.

Results

Synaptotagmin I C2A and C2AB preferentially bind to liquid-disordered phase regions on asymmetric two-phase lipid bilayers

The preparation and geometry of asymmetric supported membranes are illustrated in Figure 1. The images in Figure 2 represent the outer leaflet (bPC/bSM (1:1) plus 20% cholesterol) monolayers (green images) containing co-existing l_o and l_d phases and the bound C2 domain proteins (red images) after binding to the inner leaflet of the asymmetric lipid bilayers. By convention, “outer” and “inner” refer in this study to the lipid leaflets of a cell plasma membrane that our asymmetric supported bilayers are mimicking and not to the configuration in the supported membrane. The outer leaflet lipid mixtures formed stable l_o and l_d phases as visualized by the lipid probe NBD-DPPE, which preferentially partitions into l_o phases (39). The inner leaflet lipid mixtures contain either bPC, 15% POPS, and 20% cholesterol (Figure 2A and B) or bPC, 15% POPS, 20% cholesterol, and 1% bPIP$_2$ (Figure 2C and D)[2]. The inner leaflet monolayers were not stained in these experiments, but are known to form induced l_o phases on top of outer leaflet l_o phases through transbilayer phase coupling ((30), also see Supporting Information Figure 1, for an example).

A solution containing 0.2 μM syt I C2A (Figure 2, panels A2 and C2) or C2AB (Figure 2, panels B2 and D2) in HKC buffer (25 mM HEPES, 100 mM KCl, 1 mM $CaCl_2$, pH 7.4) was injected into the sample chamber to saturate the whole bilayer area. The binding process was monitored by TIRFM, and the protein images were taken 20 to 30 mins after injection. The

[2]Similar C2 domain binding data as presented throughout this study were also obtained with bPS instead of POPS, but the results were generally more consistent with POPS (smaller standard errors) than with bPS in the inner leaflets (data not shown). Generally, the same conclusions can be drawn with both lipids.

C2A and C2AB images are reversed in contrast when compared to the NBD-DPPE images of the outer leaflet monolayers. Therefore, both C2A and C2AB bind to inner leaflet monolayers preferentially in the more disordered lipid phase regions. This selective binding of C2A and C2AB was observed for all inner leaflet lipid mixtures that were investigated in this study, but the binding ratios varied depending on conditions as described further below.

Calcium-independent binding of synaptotagmin I C2AB

In the absence of Ca^{2+}, syt I C2A does not bind to any of these asymmetric bilayers containing anionic phospholipids. In marked contrast, syt I C2AB binds to such asymmetric bilayers in the absence of Ca^{2+} most likely through the interaction of the polybasic region of C2B with the anionic phospholipids (21). Although we performed most of the experiments of this study as described above for Figure 2, no lipid dyes were included in the bilayers for the ratiometric experiments described below. We found that this refinement yielded more accurate protein binding ratios because it required no correction for bleed-through from NBD-DPPE fluorescence in the 540 nm channel.

Figure 3 shows the syt I C2AB fluorescence intensity ratios of l_o domain regions over l_d non-domain regions after binding to asymmetric planar supported lipid bilayers in the absence of Ca^{2+} (1 mM EGTA). The outer leaflets of these experiments contained bPC/bSM (1:1) plus 20% cholesterol. The inner leaflets contained either bPC and 20% cholesterol plus different concentrations of POPS with or without bPE (bPC/bPE = 1:1) (Figure 3A), or bPC, 15% POPS, and 20% cholesterol plus different concentrations of $bPIP_2$ (Figure 3B). The mean fluorescence intensity ratios were around 0.5 and did not significantly depend on inner leaflet lipid compositions. It has been shown that when the polybasic region of C2B interacts electrostatically with anionic phospholipids in the absence of Ca^{2+}, it does not penetrate into the membrane (21). This means that the calcium-independent binding of syt I C2AB depends on the charge density on the inner leaflet lipid surface and is less sensitive to specific lipid compositions. Therefore and assuming that the valence on the protein is not changed by the different lipid phases, our results show that the charge density on the l_d phase areas is significantly higher as that on the l_o phase areas. Figure 3 also indicates that the overall charge distribution between l_o and l_d phases does not depend on the specific acidic lipid PS and PIP_2 concentrations and is independent of the presence or absence of the other major uncharged inner leaflet lipid PE.

Synaptotagmin I C2 domain binding to asymmetric two-phase bilayers composed of different concentrations of PS and PE

Figure 4 shows syt I C2A (Figure 4A) and C2AB (Figure 4B) fluorescence intensity ratios of l_o domain regions over l_d non-domain regions after binding to asymmetric two-phase lipid bilayers in the presence of 1 mM Ca^{2+}. All outer leaflets contained bPC/bSM (1:1) plus 20% cholesterol. The inner leaflets contained bPC, 15% or 40% POPS, and 20% cholesterol, with or without bPE (bPC/bPE = 1:1).

No significant differences in the mean intensity ratios were observed after binding of C2A to inner leaflet monolayers containing 15% or 40% PS. The ratios were still close to 0.5, indicating that Ca^{2+}-mediated binding did not redistribute PS between the ordered and disordered phases. Again, twice as much C2A bound to the l_d compared to the l_o phase regions. However, C2AB bound better to l_o phase regions than C2A and this effect was more pronounced at 40% than at 15% PS. The mean fluorescence intensity ratios were 0.59 (15% PS) or 0.71 (40% PS), indicating that compared to C2A more C2AB bound to the l_o phase and that the enhancement of l_d over l_o phase binding of C2AB was only 1.7 and 1.4 fold at 15 and 40% PS, respectively. Adding bPE to inner leaflet monolayers largely reversed this effect and restored the enhancement to about 2 fold. These results suggest that

binding of C2AB to ordered regions of PC membranes is enhanced at high PS concentrations compared to binding of C2A. However, this binding enhancement does not take place in equimolar PC/PE membranes with high concentrations of PS. A possible explanation for this effect is that PEs, which have higher chain melting phase transitions than equivalent PCs, do not allow for a similar penetration of C2AB domains in the ordered phase and/or may not allow for protein-induced redistribution of PS in favor of the ordered phase like a PC bilayer does.

Synaptotagmin I C2 domain binding to asymmetric two-phase bilayers composed of different concentrations of PIP_2

In Figures 2C and D we presented images of C2A and C2AB binding to two-phase bilayers containing 1% PIP_2 in addition to 15% PS. Figure 5 shows syt I C2A (Figure 5A) and C2AB (Figure 5B) fluorescence intensity ratios of l_o domain regions over l_d non-domain regions after binding to asymmetric two-phase lipid bilayers in the presence of 1 mM Ca^{2+} and with various amounts of PIP_2 included. All the outer leaflets contained bPC/bSM (1:1) plus 20% cholesterol while the inner leaflets contained bPC, 15% POPS, 20% cholesterol plus 0 to 5% $bPIP_2$. Compared to the PS-containing bilayers without PIP_2, the l_o/l_d phase partitioning of C2A shifted by about 20% and 40% less C2A bound to the l_o phase regions when 1% or 5% PIP_2 were added, respectively. At 1% PIP_2, C2A is up to 2.3 times more likely to be found in the l_d than in the l_o phase, but at 5% PIP_2, this factor increases to 3.1. Since we have already established with C2AB binding to these membranes in the absence of Ca^{2+} that the balance of PS and PIP_2 partitioning between l_o and l_d phases is independent of the PIP_2 concentration (Figure 3B), the enhanced binding of C2A is most likely due to more C2A binding to the higher concentrations of PIP_2 present in the l_d than in the l_o phase. Moreover, even more PIP_2 may accumulate in the l_d phase as a result of protein binding and could additionally contribute to the increased binding to this phase. Interestingly, C2AB binding to the l_o phase regions increased by 6-7% when 1 or 5% PIP_2 was added. As was the case with PS, C2AB in the presence of Ca^{2+} seems to have a higher affinity for l_o phases than C2A and therefore may tip the balance to more PIP_2 partitioning into l_o phases than is the case after C2A binding to phase-separated lipid membranes of the same compositions.

Discussion

Eighty five years ago, Gorter and Grendel discovered in pioneering work that biological membranes are formed by lipid bilayers (40). Forty seven years later, Singer and Nicolson introduced the “fluid mosaic model”, in which the plasma membrane is regarded as a two-dimensional solution of freely diffusing membrane proteins embedded in a fluid lipid bilayer (41). In this model, the bilayer is considered to be a uniform, semi-permeable barrier that serves as a passive homogeneous fluid matrix for membrane proteins. However, after extensive research on the dynamics and organization of plasma and organellar membranes, biological membranes are now considered to be much more organized and laterally heterogeneous than previously thought. A popular explanation for this inhomogeneity is the existence of lipid micro- or nano-domains in cellular membranes that are sometimes also referred to as lipid “rafts” (42, 43). The physical properties and biological functions of these domains have received significant attention over the last fifteen years. Lipid rafts have been equated with detergent resistant biochemical membrane fractions (DRMs) and have been proposed to be involved in a wide variety of important cellular processes, particularly in signal transduction, membrane protein sorting, membrane trafficking, and the budding of viral particles from cell surfaces (44).

More than 200 membrane proteins have been found in DRMs (45) and various SNARE proteins have been included in this list (46, 47). However, other interpretations of cholesterol-dependent cluster formation of SNAREs have been proposed (28, 29, 48). When

SNAREs were reconstituted in coexisting l_o and l_d phase giant unilamellar vesicles, they partitioned favorably into the l_d phase regions (49). Therefore, it appears that SNAREs may actually be excluded from cholesterol-rich membrane regions. SNAREs and synaptotagmin I are cooperating in Ca^{2+}-regulated membrane fusion in neurosecretion. Following the commonly accepted model that syt I functions by binding at least with its C2B domain to the presynaptic membrane it may be efficient to target its C2 domains to the same membrane domains as the SNAREs at nascent fusion sites at the synapse. Since the synaptic vesicle protein syt I interacts via one or both of its C2 domains only with the cytoplasmic leaflets of the presynaptic plasma or vesicle membranes, it does not encounter lipid mixtures that form large rafts in vitro (PC, SM and cholesterol), because these lipids are mostly localized in the outer leaflets of plasma membranes (50). As shown in this study, C2 domains indeed interact preferentially with the more disordered (non-raft) inner leaflet regions of asymmetric lipid model membranes. Therefore, they are targeted to the same regions of the membrane as SNAREs, thereby enhancing the likelihood that these molecules are co-localized and act together in the cell.

To our knowledge, this is the first time that the l_o/l_d phase domain targeting of an electrostatically bound and partially membrane-penetrating membrane protein has been studied on an inner leaflet raft lipid mixture. The method should of course be valid for studying the targeting of many other peripheral inner leaflet membrane proteins. A plethora of intracellular signaling domains interact with plasma membranes in this fashion and it will be very interesting to see how they partition between different lipid phases and whether they actually fulfill a central tenet of the raft hypothesis of transmembrane signal transduction, which is that they should co-partition into the same lipid domains of the plasma membrane as extracellular receptors after stimulation with appropriate ligands.

The supported asymmetric two-phase lipid bilayer system (30, 32) that we used here has several advantages that make it attractive for these studies. First, the bilayers have asymmetric lipid distributions, which closely mimic those in plasma membranes and which are difficult to achieve in other model membrane systems. The major lipid components from outer (PC, SM and cholesterol) and inner (PC, PE, PS, PI and cholesterol) leaflets of plasma membranes can be used pretty much at will to form the first and second monolayers of the supported bilayers, respectively. We have discovered previously that co-existing l_o and l_d phases in outer leaflet lipid mixtures can induce the l_o-l_d phase separation in adjacent inner leaflet lipids by transbilayer phase coupling (30, 32). Second, by changing the inner leaflet lipid compositions in the regions of co-existing l_o and l_d phases as done in the present study, we can separate protein-lipid interactions that are lipid-specific (e.g. interactions with a specific acidic lipid) from those that are lipid phase-specific. Of course, these two types of interaction are not always independent as has been the case with the C2 domains studied here, but at least the interactions can be studied separately in the two co-existing phases. Most bulk methods that are currently in use cannot make this distinction. And third, the planar geometry of supported bilayers facilitates microscopic observations and interpretation of the images because no curvature effects need to be considered.

As with every new method, there are of course also disadvantages. Questions persist as to whether the solid support has any influence on the phase behavior of the supported bilayer. We tried to minimize this influence by using a 4 nm polymer cushion between the solid support and bilayer (51). Despite this cushion, which allows for free diffusion of the lipids and some proteins in both leaflets of the bilayer, the domains as a whole are not moving in this system. They are probably “pinned” in a few places to protrusions or other imperfections on the solid support. Thus even though we believe that the support-membrane interactions are quite minimal, they are not completely eliminated in this system. Despite this caveat, the exposed inner leaflet surface may not be significantly perturbed by this

pinning. Studies with free-standing asymmetric two-phase bilayers in “black lipid membranes” also have found phase coupling between l_o and l_d phase regions across the mid-plane of the bilayer (52), i.e. confirming conclusions drawn from our supported membrane approach. No inner leaflet protein targeting experiments have yet been reported in black lipid membranes. Asymmetric membranes may also be produced by lipid exchange in relatively small unilamellar vesicles (53). However, these vesicles are too small to optically resolve possible phase separations and therefore are not suitable to study localized membrane protein targeting as conducted here.

In the current study, we have focused on binding ratios between l_o and l_d phase regions. We also attempted to obtain absolute binding to individual domain regions in the course of these studies, but found this to be more difficult. Absolute fluorescence intensities are not well calibrated on a TIRF microscope, which makes it difficult to compare experiments performed on different bilayers and different days. There may be ways to remedy this problem with appropriate internal standards in the future, but differences that we observed in individual binding behaviors require careful analysis and confirmation.

Because we observe similar results for binding of C2AB to PS-containing membranes in the absence of Ca^{2+} and C2A in the presence of calcium, we think that the PS distribution between these two phases dominates the binding reaction and that these proteins under these conditions may be good reporters of PS partitioning between the two phases. C2AB binding in the absence of Ca^{2+} may be particularly suitable for this purpose because its binding is thought to be purely electrostatic and is not confounded with loop penetration into hydrophobic portions of the bilayer (21). It will be interesting to see whether this method can be further developed in the future as a reliable probe of acidic lipid partitioning between different lipid phases. More systematic studies along these lines and a more thorough analysis in terms of the electrostatic surface potential on binding will be required to further develop this method into a truly quantitative tool for measuring acidic lipid partitioning.

Our result that C2A binds in the presence of Ca^{2+} very strongly to PIP_2 in the l_d phase is not surprising. Brain PIP_2 has highly unsaturated acyl chains and therefore likely partitions well into the l_d phase. Since PIP_2 bears a negative charge of −3 to −4 at neutral pH, it is expected to strongly electrostatically attract Ca^{2+}-C2A. C2A also partially penetrates into the hydrophobic interior of the bilayer, which should be facilitated by the more disordered l_d phase compared to the more ordered l_o phase. These two factors may cooperate as the overall PIP_2 concentration is increased in the membrane and thereby further shift this lipid's partition equilibrium to the l_d phase at high PIP_2 concentrations. Interestingly, this cooperative effect is not observed with C2AB. C2AB clearly has a higher affinity for the l_o phase than C2A. The opposing forces of greater PIP_2 partitioning into the l_d phase and the higher relative affinity of C2AB towards the l_o phase probably cancel the fluidity-electrostatic cooperativity that has been seen with C2A and could explain the observed difference between the behaviors of C2A and C2AB in these lipid systems.

In summary, this study of acidic lipid targeting of synaptotagmin I C2 domains to membrane regions of different lipid acyl chain order provided fundamental new insight on how acidic lipids distribute between ordered and disordered regions of the inner leaflet in heterogeneous asymmetric lipid bilayers. It also provided fundamental new information on how synaptotagmin I may target heterogeneously structured lipid surfaces of plasma membranes from within cells. Importantly, syt I and PIP_2 appear to be targeted to similar membrane regions as the SNAREs. This should increase the probability of encounter and functional interaction of SNAREs, syt I, PIP_2 and Ca^{2+} in these regions. The membrane therefore likely acts as an organizing medium bringing several of the most critical components together, which are all known players in Ca^{2+}-triggered exocytosis by membrane fusion in

neuroendocrine cells. This principle of organizing functionally related membrane components in similar locations in the membrane may not be limited to membrane fusion, but could also operate in other membrane-assembled molecular machines or membrane-assisted systems of signal transduction.

Supplementary Material

Refer to Web version on PubMed Central for supplementary material.

Acknowledgments

With thank Dr. Michael Wiener for his interest and helpful comments in the course of this work. We also thank members of the Tamm laboratory for many helpful discussions. This work was supported by NIH grant P01 GM072694.

References

1. Jahn R, Lang T, Sudhof TC. Membrane fusion. Cell. 2003; 112:519–533. [PubMed: 12600315]
2. Rizo J, Rosenmund C. Synaptic vesicle fusion. Nat Struct Mol Biol. 2008; 15:665–674. [PubMed: 18618940]
3. Sudhof TC, Rothman JE. Membrane fusion: grappling with SNARE and SM proteins. Science. 2009; 323:474–477. [PubMed: 19164740]
4. Brunger AT. Structure and function of SNARE and SNARE-interacting proteins. Q Rev Biophys. 2005; 38:1–47. [PubMed: 16336742]
5. Fasshauer D. Structural insights into the SNARE mechanism. Biochim Biophys Acta. 2003; 1641:87–97. [PubMed: 12914950]
6. Jahn R, Scheller RH. SNAREs--engines for membrane fusion. Nat Rev Mol Cell Biol. 2006; 7:631–643. [PubMed: 16912714]
7. McNew JA. Regulation of SNARE-mediated membrane fusion during exocytosis. Chem Rev. 2008; 108:1669–1686. [PubMed: 18419164]
8. Sollner TH. Regulated exocytosis and SNARE function (Review). Mol Membr Biol. 2003; 20:209–220. [PubMed: 12893529]
9. Brose N, Petrenko AG, Sudhof TC, Jahn R. Synaptotagmin: a calcium sensor on the synaptic vesicle surface. Science. 1992; 256:1021–1025. [PubMed: 1589771]
10. Chapman ER. How does synaptotagmin trigger neurotransmitter release? Annu Rev Biochem. 2008; 77:615–641. [PubMed: 18275379]
11. Fernandez-Chacon R, Konigstorfer A, Gerber SH, Garcia J, Matos MF, Stevens CF, Brose N, Rizo J, Rosenmund C, Sudhof TC. Synaptotagmin I functions as a calcium regulator of release probability. Nature. 2001; 410:41–49. [PubMed: 11242035]
12. Jackson MB, Chapman ER. Fusion pores and fusion machines in Ca2+-triggered exocytosis. Annu Rev Biophys Biomol Struct. 2006; 35:135–160. [PubMed: 16689631]
13. Perin MS, Fried VA, Mignery GA, Jahn R, Sudhof TC. Phospholipid binding by a synaptic vesicle protein homologous to the regulatory region of protein kinase C. Nature. 1990; 345:260–263. [PubMed: 2333096]
14. Perin MS, Brose N, Jahn R, Sudhof TC. Domain structure of synaptotagmin (p65). J Biol Chem. 1991; 266:623–629. [PubMed: 1985919]
15. Fernandez I, Arac D, Ubach J, Gerber SH, Shin O, Gao Y, Anderson RG, Sudhof TC, Rizo J. Three-dimensional structure of the synaptotagmin 1 C2B-domain: synaptotagmin 1 as a phospholipid binding machine. Neuron. 2001; 32:1057–1069. [PubMed: 11754837]
16. Ubach J, Zhang X, Shao X, Sudhof TC, Rizo J. Ca2+ binding to synaptotagmin: how many Ca2+ ions bind to the tip of a C2-domain? Embo J. 1998; 17:3921–3930. [PubMed: 9670009]
17. Martens S, McMahon HT. Mechanisms of membrane fusion: disparate players and common principles. Nat Rev Mol Cell Biol. 2008; 9:543–556. [PubMed: 18496517]

18. Chapman ER, Davis AF. Direct interaction of a Ca2+-binding loop of synaptotagmin with lipid bilayers. J Biol Chem. 1998; 273:13995–14001. [PubMed: 9593749]
19. Herrick DZ, Sterbling S, Rasch KA, Hinderliter A, Cafiso DS. Position of synaptotagmin I at the membrane interface: cooperative interactions of tandem C2 domains. Biochemistry. 2006; 45:9668–9674. [PubMed: 16893168]
20. Rufener E, Frazier AA, Wieser CM, Hinderliter A, Cafiso DS. Membrane-bound orientation and position of the synaptotagmin C2B domain determined by site-directed spin labeling. Biochemistry. 2005; 44:18–28. [PubMed: 15628842]
21. Kuo W, Herrick DZ, Ellena JF, Cafiso DS. The calcium-dependent and calcium-independent membrane binding of synaptotagmin 1: two modes of C2B binding. J Mol Biol. 2009; 387:284–294. [PubMed: 19302798]
22. Bai J, Tucker WC, Chapman ER. PIP2 increases the speed of response of synaptotagmin and steers its membrane-penetration activity toward the plasma membrane. Nat Struct Mol Biol. 2004; 11:36–44. [PubMed: 14718921]
23. Bai J, Wang P, Chapman ER. C2A activates a cryptic Ca(2+)-triggered membrane penetration activity within the C2B domain of synaptotagmin I. Proc Natl Acad Sci U S A. 2002; 99:1665–1670. [PubMed: 11805296]
24. Cafiso, DS. Structure and Interactions of C2 Domains at Membrane Surfaces. Wiley-VCH; Weinheim, Germany: 2005.
25. Martens S, Kozlov MM, McMahon HT. How synaptotagmin promotes membrane fusion. Science. 2007; 316:1205–1208. [PubMed: 17478680]
26. Lee HK, Yang Y, Su Z, Hyeon C, Lee TS, Lee HW, Kweon DH, Shin YK, Yoon TY. Dynamic Ca2+-dependent stimulation of vesicle fusion by membrane-anchored synaptotagmin 1. Science. 2010; 328:760–763. [PubMed: 20448186]
27. Stein A, Radhakrishnan A, Riedel D, Fasshauer D, Jahn R. Synaptotagmin activates membrane fusion through a Ca2+-dependent trans interaction with phospholipids. Nat Struct Mol Biol. 2007; 14:904–911. [PubMed: 17891149]
28. Lang T, Bruns D, Wenzel D, Riedel D, Holroyd P, Thiele C, Jahn R. SNAREs are concentrated in cholesterol-dependent clusters that define docking and fusion sites for exocytosis. Embo J. 2001; 20:2202–2213. [PubMed: 11331586]
29. Ohara-Imaizumi M, Nishiwaki C, Kikuta T, Kumakura K, Nakamichi Y, Nagamatsu S. Site of docking and fusion of insulin secretory granules in live MIN6 beta cells analyzed by TAT-conjugated anti-syntaxin 1 antibody and total internal reflection fluorescence microscopy. J Biol Chem. 2004; 279:8403–8408. [PubMed: 14676208]
30. Wan C, Kiessling V, Tamm LK. Coupling of cholesterol-rich lipid phases in asymmetric bilayers. Biochemistry. 2008; 47:2190–2198. [PubMed: 18215072]
31. Wang TY, Silvius JR. Cholesterol does not induce segregation of liquid-ordered domains in bilayers modeling the inner leaflet of the plasma membrane. Biophys J. 2001; 81:2762–2773. [PubMed: 11606289]
32. Kiessling V, Crane JM, Tamm LK. Transbilayer effects of raft-like lipid domains in asymmetric planar bilayers measured by single molecule tracking. Biophys J. 2006; 91:3313–3326. [PubMed: 16905614]
33. Frazier AA, Roller CR, Havelka JJ, Hinderliter A, Cafiso DS. Membrane-bound orientation and position of the synaptotagmin I C2A domain by site-directed spin labeling. Biochemistry. 2003; 42:96–105. [PubMed: 12515543]
34. Crane JM, Kiessling V, Tamm LK. Measuring lipid asymmetry in planar supported bilayers by fluorescence interference contrast microscopy. Langmuir. 2005; 21:1377–1388. [PubMed: 15697284]
35. Kalb E, Frey S, Tamm LK. Formation of supported planar bilayers by fusion of vesicles to supported phospholipid monolayers. Biochim Biophys Acta. 1992; 1103:307–316. [PubMed: 1311950]
36. Wagner ML, Tamm LK. Tethered polymer-supported planar lipid bilayers for reconstitution of integral membrane proteins: silane-polyethyleneglycol-lipid as a cushion and covalent linker. Biophys J. 2000; 79:1400–1414. [PubMed: 10969002]

37. Oreopoulos J, Yip CM. Combinatorial microscopy for the study of protein-membrane interactions in supported lipid bilayers: Order parameter measurements by combined polarized TIRFM/AFM. J Struct Biol. 2009; 168:21–36. [PubMed: 19268707]
38. Kiessling V, Domanska MK, Tamm LK. Single SNARE-mediated vesicle fusion observed in vitro by polarized TIRFM. Biophys J. 2010; 99:4047–4055. [PubMed: 21156148]
39. Crane JM, Tamm LK. Role of cholesterol in the formation and nature of lipid rafts in planar and spherical model membranes. Biophys J. 2004; 86:2965–2979. [PubMed: 15111412]
40. Gorter E, Grendel F. On Bimolecular Layers of Lipoids on the Chromocytes of the Blood. J Exp Med. 1925; 41:439–443. [PubMed: 19868999]
41. Singer SJ, Nicolson GL. The fluid mosaic model of the structure of cell membranes. Science. 1972; 175:720–731. [PubMed: 4333397]
42. London E. How principles of domain formation in model membranes may explain ambiguities concerning lipid raft formation in cells. Biochim Biophys Acta. 2005; 1746:203–220. [PubMed: 16225940]
43. Simons K, Ikonen E. Functional rafts in cell membranes. Nature. 1997; 387:569–572. [PubMed: 9177342]
44. Lingwood D, Simons K. Lipid rafts as a membrane-organizing principle. Science. 2010; 327:46–50. [PubMed: 20044567]
45. Foster LJ, De Hoog CL, Mann M. Unbiased quantitative proteomics of lipid rafts reveals high specificity for signaling factors. Proc Natl Acad Sci U S A. 2003; 100:5813–5818. [PubMed: 12724530]
46. Chamberlain LH, Burgoyne RD, Gould GW. SNARE proteins are highly enriched in lipid rafts in PC12 cells: implications for the spatial control of exocytosis. Proc Natl Acad Sci U S A. 2001; 98:5619–5624. [PubMed: 11331757]
47. Salaun C, Gould GW, Chamberlain LH. Lipid raft association of SNARE proteins regulates exocytosis in PC12 cells. J Biol Chem. 2005; 280:19449–19453. [PubMed: 15769746]
48. Murray DH, Tamm LK. Clustering of syntaxin-1A in model membranes is modulated by phosphatidylinositol 4,5-bisphosphate and cholesterol. Biochemistry. 2009; 48:4617–4625. [PubMed: 19364135]
49. Bacia K, Schuette CG, Kahya N, Jahn R, Schwille P. SNAREs prefer liquid-disordered over “raft” (liquid-ordered) domains when reconstituted into giant unilamellar vesicles. J Biol Chem. 2004; 279:37951–37955. [PubMed: 15226320]
50. Kiessling V, Wan C, Tamm LK. Domain coupling in asymmetric lipid bilayers. Biochim Biophys Acta. 2009; 1788:64–71. [PubMed: 18848518]
51. Kiessling V, Tamm LK. Measuring distances in supported bilayers by fluorescence interference-contrast microscopy: polymer supports and SNARE proteins. Biophys J. 2003; 84:408–418. [PubMed: 12524294]
52. Collins MD, Keller SL. Tuning lipid mixtures to induce or suppress domain formation across leaflets of unsupported asymmetric bilayers. Proc Natl Acad Sci U S A. 2008; 105:124–128. [PubMed: 18172219]
53. Cheng HT, Megha, London E. Preparation and properties of asymmetric vesicles that mimic cell membranes: effect upon lipid raft formation and transmembrane helix orientation. J Biol Chem. 2009; 284:6079–6092. [PubMed: 19129198]

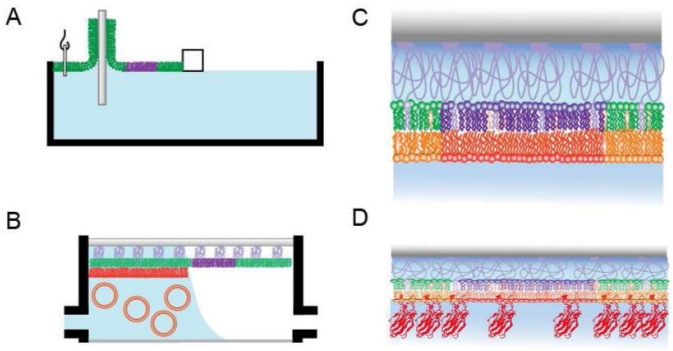

FIGURE 1.

Preparation of asymmetric two-phase supported bilayers and protein binding. (A) Langmiur-Blodgett (LB) film deposition: The lipid mixture containing bPC/bSM/cholesterol/polymer is spread on the air-water interface and compressed to form a lipid monolayer. The quartz substrate is rapidly dipped and slowly raised through this interface. A constant surface pressure is maintained through computer feedback during this process. (B) Vesicle fusion (VF): The LB-coated quartz slide is placed in a custom built flow-through chamber. A LUV solution is slowly and carefully injected into the chamber and allowed to spontaneously fuse with the LB monolayer. Excess vesicles are then washed out by extensive buffer rinsing. (C) Single planar polymer-supported bilayer formed from l_o-phase-inducing lipid combinations in (A) and (B). (D) Binding of synaptotagmin I C2A or C2AB domains after perfusion and washing of the chamber with a preformed asymmetric bilayer.

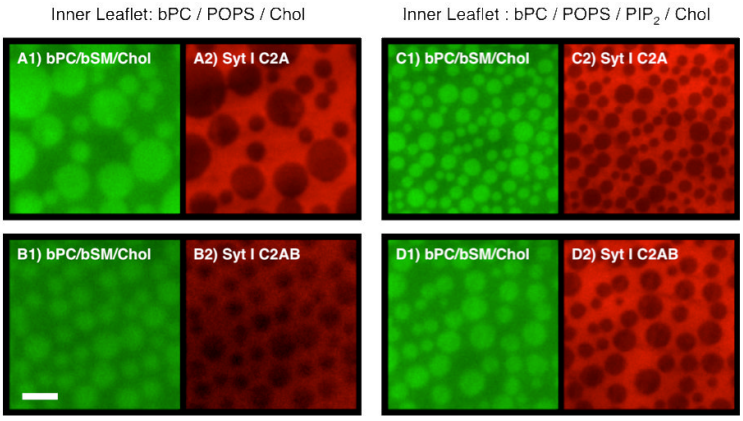

FIGURE 2.

Representative images of Ca^{2+}-mediated synaptotagmin I C2A and C2AB domain binding to asymmetric two-phase bilayers with outer leaflet monolayers composed of bPC/bSM (1:1) plus 20% cholesterol and supported on a polymer cushion and inner leaflet monolayers composed of bPC, 15% POPS and 20% cholesterol (left panels) or bPC, 15% POPS, 1% $bPIP_2$ and 20% cholesterol (right panels). The outer leaflet monolayers are visualized with 0.25% NBD-DPPE, which preferentially partitions into l_o phases (green images). The inner leaflet monolayers are not labeled, but are known to form induced l_o phases on top of outer leaflet l_o phases (30). Alexa-546 labeled synaptotagmin I C2A (top panels) and C2AB (bottom panels) domains bind to induced inner leaflet l_o and l_d phase domains, and preferentially partition to the more disordered lipid phase regions (red images). Scale bar: 10 μm.

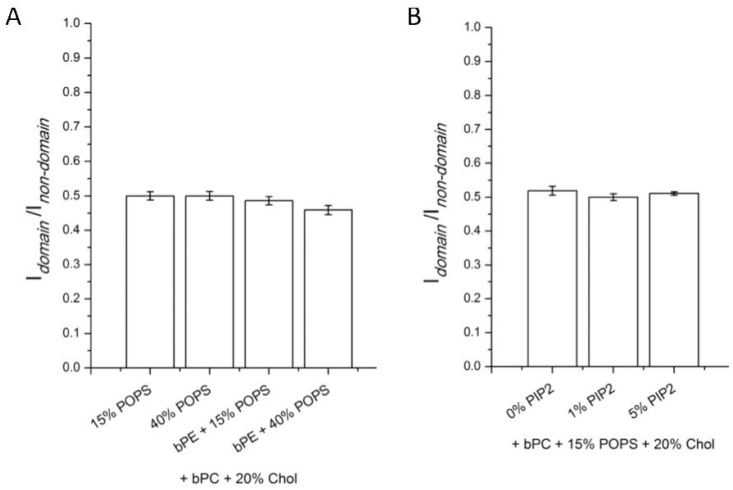

FIGURE 3.

Synaptotagmin I C2AB fluorescence intensity ratios of ordered lipid domain regions over disordered lipid non-domain regions after binding to asymmetric two-phase bilayers in the absence of Ca^{2+} (1 mM EGTA). The lipid compositions of the inner leaflet monolayers are as labeled on the x-axis. All outer leaflet monolayers are composed of bPC/bSM (1:1) plus 20% cholesterol and supported on a polymer cushion. (A) Binding and fluorescence ratios to inner leaflet monolayer with different concentrations of PS and PE. bPC/bPE is 1:1 when bPE is present. (B) Binding and fluorescence ratios to inner leaflet monolayer with different concentrations of PIP_2 in the presence of 15% PS. Error bars indicate standard errors.

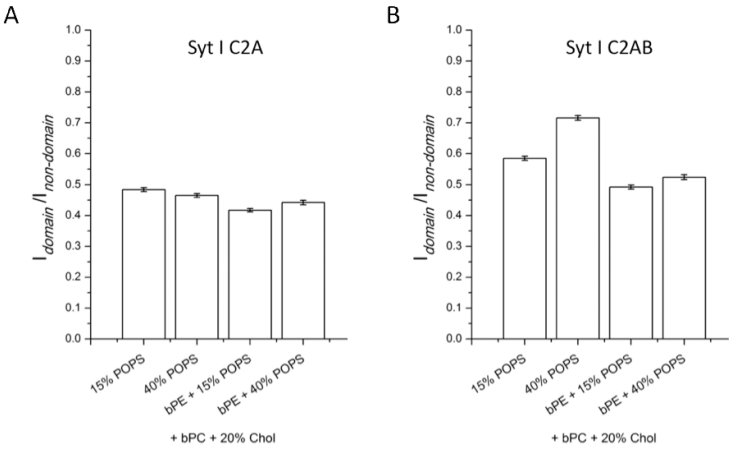

FIGURE 4.

Synaptotagmin I C2A (A) and C2AB (B) fluorescence intensity ratios of ordered lipid domain regions over disordered lipid non-domain regions after binding to asymmetric two-phase bilayers in the presence of 1 mM Ca^{2+}. The inner leaflet monolayers contain different concentrations of PS and PE as indicated on the x-axis. bPC/bPE is 1:1 when bPE is present. All outer leaflet monolayers are composed of bPC/bSM (1:1) plus 20% cholesterol and supported on a polymer cushion. Error bars indicate standard errors.

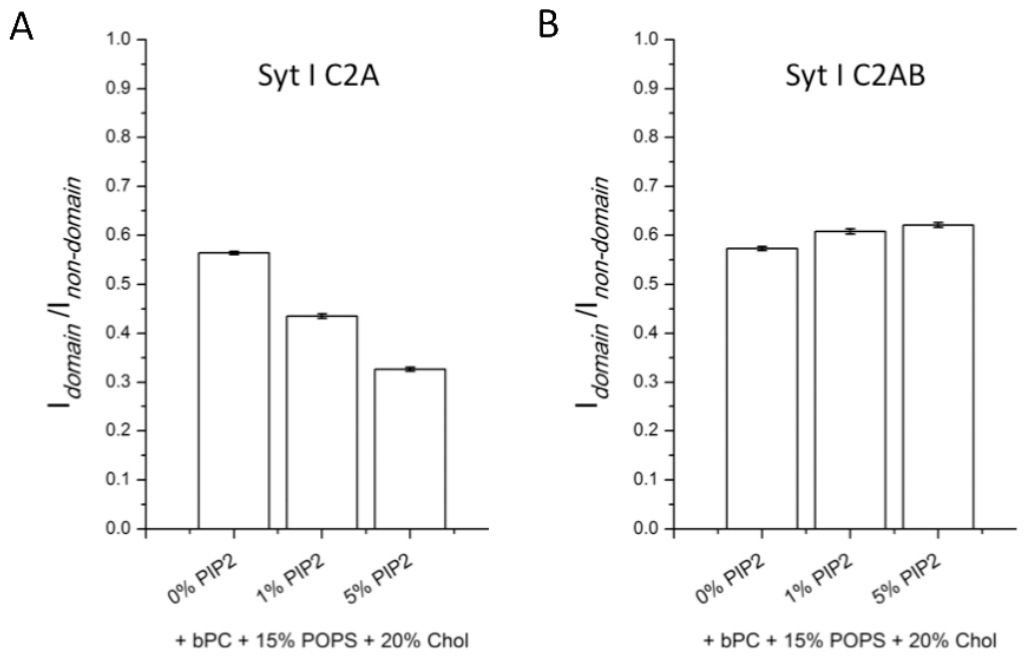

FIGURE 5.

Synaptotagmin I C2A (A) and C2AB (B) fluorescence intensity ratios of ordered lipid domain regions over disordered lipid non-domain regions after binding to asymmetric two-phase bilayers in the presence of 1 mM Ca^{2+} and increasing concentrations of $bPIP_2$ in the inner leaflet monolayers as indicated on the x-axis. All outer leaflet monolayers are composed of bPC/bSM (1:1) plus 20% cholesterol and supported on a polymer cushion. Error bars indicate standard errors.